Front. Phys. China, 2008, 3(4): 436–443
DOI 10.1007/s11467-008-0037-8

RESEARCH ARTICLE

Yong HAN

A jellium model analysis on quantum growth of metal nanowires and nanomesas

Abstract A simple jellium model is used to investigate the stability of a metal nanowire as a function of its size. The theoretical results from the model indicate the quantum selectivity of preferable radii of nanowires, in apparent agreement with the experimental observations. It is consequently suggested that a series of stable "magic numbers" and "instability gaps" observed in the synthesis experiments of Au nanowires is mainly attributed to the quantum-mechanical behavior. These stable radii can be achieved by rearranging atoms during the formation of nanowires. The model is also used to analyze the growth of Au nanomesas on a graphite surface, and the puzzling growth behavior of Au nanomesas can be reasonably explained.

Keywords jellium model, free electrons, quantum size effects, metal nanowires, metal nanomesas

PACS numbers 81.10.Aj, 81.07.-b, 61.46.-w, 36.40.Qv

1 Introduction

A metal nanostructure often exhibits a size-dependent feature arising from quantum confinement when its structural dimension is comparable to the electron Fermi wavelength, a phenomenon referred to as the quantum size effect (QSE). The QSE can have two distinct size-dependent manifestations: a property anomaly at certain selected size, i.e., the so-called "magic" size, or an oscillatory size-dependent property. For example, metal nanoclusters are anomalously stable when they contain a magic number of atoms [1−5]; a chain of transition metal atoms shows an oscillatory magnetic moment with increasing chain length [6]; and, metal nanofilms display a periodic oscillation of stability with increasing film thickness [7, 8]. The size-dependency of physical properties of metal nanostructures has attracted much interest because it is of importance not only in fundamental physics but also in many targeted potential applications, e.g., electronic device technology, nanocatalysts, sensors, biological interfaces, and functional materials. However, the measurement and interpretation of properties relevant to metal nanostructures manifests a considerable theoretical and experimental challenge [2−5] because, as mentioned above, the big difference in properties often exists between a metal nanostructure and its bulk counterpart.

Nanowires, belonging to one type of nanostructure, can be produced by employing various experimental techniques that have burgeoned in the past decade. Such experiments on alkali metals [9−11], noble metals [12−14], Al [15−17], and Bi [18] have revealed an oscillatory behavior in nanowire electrical conductivity as a function of its diameter. Suspended Au nanowires formed in an ultra-high vacuum have been reported as exhibiting a series of stable "magic numbers" and "instability gaps" [19]. Although some theoretical analyses on metal nanowires have been made to connect this magic sequence to the electron shell structure, the physical origin is still not very clear [16, 20−25].

Nanomesas, belonging to another type of nanostructure, can grow on a semiconductor or insulator surface in vacuum evaporation-deposition experiments, and often adopt a flat-top cylinder-like shape. Some puzzling

Yong HAN[1,2](✉)

[1] Department of Materials Science and Engineering, University of Utah, Salt Lake City, UT 84112, USA
[2] Current address: IPRT and Ames Laboratory, U. S. Department of Energy, 307D Wilhelm Hall, Ames, IA50011, USA
E-mail: octavian2009@gmail.com

Received April 8, 2008; accepted May 23, 2008

size-dependent growth features have been observed for metal nanomesas. For example, by depositing Au onto a surface of highly oriented pyrolytic graphite (HOPG), the Au nanomesas are formed around the surface defects [26−29]. These Au nanomesas initially grow in both height and radius. However, with increasing amount of deposited Au, the height growth of Au nanomesas is gradually hindered, and radial growth becomes predominantly favored [26]. These growth behaviors are speculated to originate from the QSE, but the corresponding theoretical study is still lacking.

In this article, a simple cylindrical hard-wall jellium model (CHWJM) combined with a chemical potential analysis is used to study Au nanowires and nanomesas. The results from the model show that the radius of a Au nanowire is of quantum selectivity, being fairly consistent with the "magic numbers" and "instability gaps" observed in the experiments of Kondo *et al.* [19] Consequently, it is suggested that the size selection of metal nanowires is mainly governed by the QSE during their formation, while a nanowire must conform to these quantum-mechanically allowable magic radii by rearranging its inner atoms. In addition, the quantum-confinement effect along the axial direction for the nanowires with different lengths are discussed. The model is also used to analyze the Au nanomesas on the HOPG surface, and the above-mentioned puzzling growth behavior of Au nanomesas can be reasonably explained.

2 Model

It has been shown that the QSE in small metal clusters can be effectively described within the framework of a jellium model, given a potential well with an even simple geometry. For example, Knight *et al.* [30] explained the mass spectra of a Na cluster, using a spherical jellium model with simple Woods-Saxon potential [31], which is initially applied to describe the main field inside a spherical atomic nucleus. Clemenger [32] investigated the possibility of ellipsoidal distortions for alkali metal clusters with Nilsson potential [33, 34], which is initially applied to describe a deformed nucleus in theoretical nuclear structure physics. Schulte [7] made a self-consistent calculation using a jellium slab, presenting a seminal theoretical prediction for the QSE in metal nanofilms. Zhang *et al.* [35, 36] have also studied metal nanofilms using the jellium slab with a simple one-dimensional rectangular potential well.

In this work, the studied system is a nanowire with a limited length or a cylinder-like nanomesa. Thus, the simplest choice for the potential is naturally the cylindrical hard-wall potential. In the present model, a nanowire or nanomesa is simplified as a jellium cylinder with radius R (diameter $D = 2R$) and length (or height) H. See Fig. 1. While the total energy of electrons can be simply analytically expressed, the CHWJM suffices in effectively capturing the essential physics of the studied problem, as discussed below.

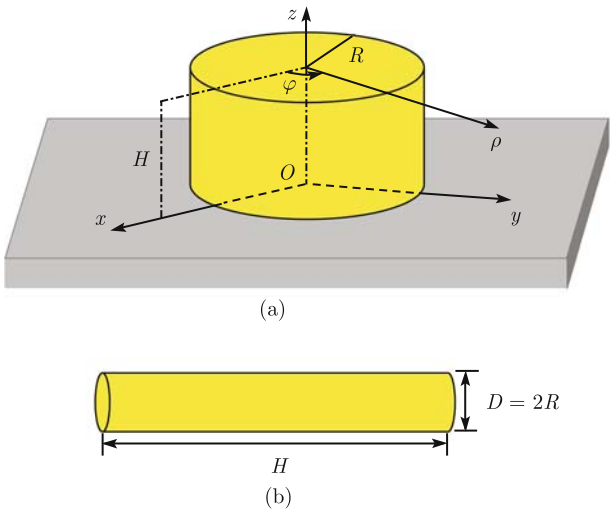

Fig. 1 Schematic illustrations of **(a)** a cylindrical nanomesa on a surface, and **(b)** a nanowire with a limited length.

For the jellium cylinder, the potential well has the general form

$$U = \begin{cases} 0, & \text{for } 0 < z < H, \text{ and } \rho < R \\ U_0, & \text{for } z < 0, z > H, \text{ or } \rho > R \end{cases} \tag{1}$$

where ρ, φ and z are the cylindrical coordinates, as shown in Fig. 1(a). It is assumed that the work function of the metal is large enough so that the potential barrier U_0 is approximately infinite, i.e., the hard-wall potential. The effects of the positive charge background from ion cores and the electron-electron interactions can be simplified by the effective mass approximation: replacing the free electron mass m_{e} with the effective mass m^*. If the interactions are neglected, m^* is simply equal to m_{e}.

The electron wavefunctions are obtained by solving the single-electron Schrödinger equation as

$$\begin{aligned} |m,\alpha,n\rangle \equiv{}& \psi_{m,\alpha,n}(\rho,\varphi,z) \\ ={}& \frac{\sqrt{2}}{R\sqrt{\pi H}J_{m+1}(Z_{m,\alpha})} \\ & \cdot J_m\left(\frac{Z_{m,\alpha}}{R}\rho\right)\mathrm{e}^{\mathrm{i}m\varphi}\sin\frac{n\pi z}{H}, \\ & m = 0, \pm1, \pm2, \cdots; \alpha = 1, 2, 3, \cdots (\alpha \neq 1, \text{if } m \neq 0); \\ & \text{and } n = 1, 2, 3, \cdots \end{aligned} \tag{2}$$

where $Z_{m,\alpha}$ is the αth zero of the Bessel function $J_m(x)$

with order m. The eigenvalues are

$$\epsilon_{m,\alpha,n} = \frac{\hbar^2}{2m^*}\left(\frac{Z_{m,\alpha}^2}{R^2} + \frac{n^2\pi^2}{H^2}\right) \tag{3}$$

By letting the N electrons occupy the lowest single-electron eigenstates, the ground-state energy of the system is simply $E = \sum_{m,\alpha,n} \epsilon_{m,\alpha,n}$, where the summation runs over all the occupied eigenstates $|m,\alpha,n\rangle$. Note that the states $|m,\alpha,n\rangle$ and $|-m,\alpha,n\rangle$ correspond to the same eigenenergy. After taking into account the spin degeneracy of each electron state, $|\pm m \neq 0,\alpha,n\rangle$ is 4-fold degenerate, and $|m=0,\alpha,n\rangle$ is 2-fold degenerate. Mills *et al.* [37] have used the above wavefunctions to study single-atom Au chains supported on a metal surface. However, they obtained an incorrect expression for wavefunctions due to the wrong normalization factor and the incomplete degeneracy of quantum number m. We think that it is necessary to clarify this by showing a strict mathematical derivation. For details, see the Appendix in this article.

3 Results and discussion

In nanowire synthesis experiments, the nanowires in their formation can become thinner or thicker due to the applied electron beam irradiation or kinetic diffusion process [19, 38]. Therefore, from the viewpoint of a jellium model, it can be assumed that the volume change of the nanowire as a jellium cylinder is "continuous" with the smallest volume unit, the Wigner-Seitz volume, which in turn is, on average, occupied by each electron. Because a change in total volume results in a corresponding change in total energy, a partial chemical potential can be introduced as [8, 39, 40]:

$$\mu_R = \left(\frac{\partial E}{\partial N}\right)_H = E_N - E_{N-1}|_{H=\text{constant}} \tag{4}$$

representing the change of energy with respect to changing the radius at a fixed length. Here, N is the total number of free electrons in the jellium cylinder. For Au, the valence electron number is one, so N is also the total number of atoms in the nanowire.

In order to describe the stability of a nanowire, a convenient method is to introduce a second different function,

$$\begin{aligned}\Delta\mu_R &= \mu_{R+\Delta R} - \mu_R \\ &= E_{N+1} - 2E_N + E_{N-1}|_{H=\text{constant}}\end{aligned} \tag{5}$$

i.e., the change in chemical potential. The system is stable if $\Delta\mu_R \geqslant 0$, and unstable if $\Delta\mu_R < 0$. If a certain radius gives rise to a relatively much larger $\Delta\mu_R$ value than its neighbors, this radius is considered to be "magically" stable. It follows that $\Delta\mu_R$ can be called the "stability index" in analyzing the stability of a nanowire as the function of its radius. This method is similar to that used in the stability analysis for alkali metal clusters [1, 30, 32].

In previous studies, a nanowire was often modelled as an infinite system [20, 41]. However, the length of an experimentally observed nanowire is always limited, e.g., the longest Au nanowires synthesized by Kondo *et al.* [19] are only 6 nm in length, and $\sim$ 11 nm by Oshima *et al.* [38] Therefore, for the purpose of comparison with these experimental results, it is necessary to calculate the nanowires using different lengths, and consequently reveal the effect of quantum confinement along the axial direction.

Figure 2 shows the calculated results of $\Delta\mu_R$ as the function of diameter D for the Au nanowires with three different lengths. It is clear that a series of stable magic radii ($\Delta\mu_R > 0$) and unstable radii ($\Delta\mu_R > 0$) appear. The data points in Fig. 2(a) are sparser in contrast to Fig. 2(b) and (c), because changing one unit volume (i.e., the Wigner-Seitz volume) will lead to a larger radial change for a shorter nanowire than for a longer nanowire. Actually, the short "nanowire" with a small length of 0.94 nm in Fig. 2(a) is more like a cylindrical cluster, which has a strong axial quantum-confinement effect, displaying a very different stability feature from those of the longer nanowires in Fig. 2(b) and (c).

Figure 2(b) shows a plot of the calculated $\Delta\mu_R$ versus diameter D for a Au nanowire 6 nm in length. A series of stable regions composed of some dense magic diameters appears around $D = 0.4$ nm, 0.58 nm, 0.75 nm, $\cdots$, respectively. There are two bigger "instability gaps", around $D = 0.47$ nm and 0.70 nm, without any stable diameters; with increasing diameter, the "instability gaps" are still observable, but become smaller and smaller. In Kondo *et al.*'s experiments [19], the histogram shows that the peaks of stable diameters are at $D = 0.58$ nm, 0.88 nm, 0.96 nm, 1.03 nm, 1.13 nm, 1.20 nm, 1.29 nm, and 1.40 nm, and no stable diameters are observed around $D = 0.50$ nm and 0.70 nm. Figure 2(c) shows a plot of the calculated $\Delta\mu_R$ versus diameter D for a Au nanowire 11.31 nm in length. Compared with Fig. 2(b), the amplitudes of $\Delta\mu_R$ in Fig. 2(c) are reduced overall, but their oscillation pattern features are quite similar, indicating that the axial quantum confinement does not strongly influence their magic diameter selectivity. From Fig. 2(b) and (c), a stable magic region should appear around $D = 0.4$ nm. This has been observed in Oshima *et al.*'s experiments [38]. Thus, for

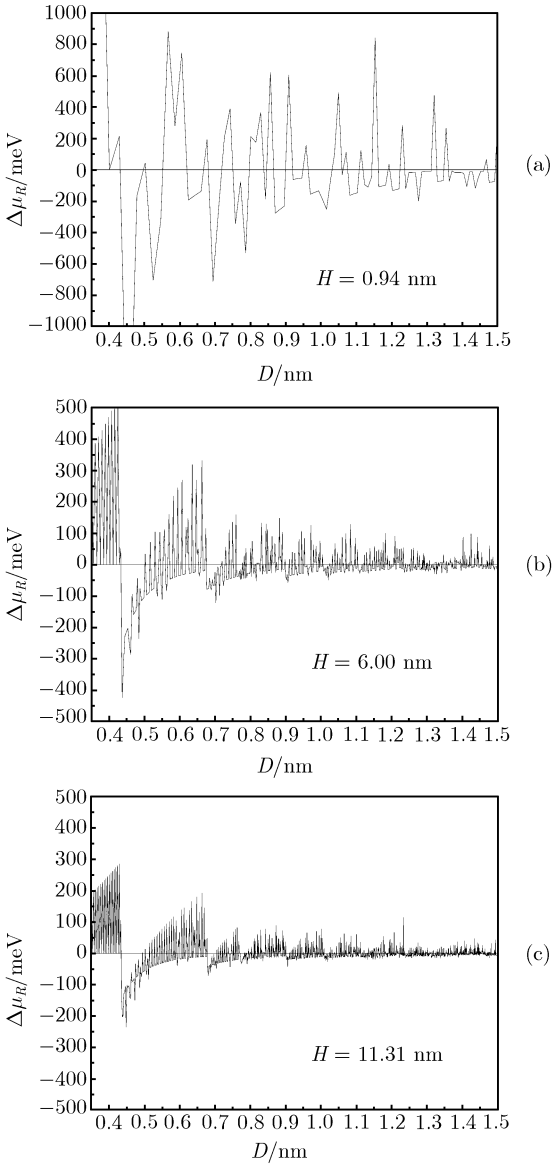

Fig. 2 Plots of $\Delta\mu_R$ versus diameter D for the Au nanowires with three different lengths: **(a)** 0.94 nm, **(b)** 6.00 nm, and **(c)** 11.31 nm.

a Au nanowire, the results from the present jellium model is in fair agreement with the existing experiments of Kondo *et al.* as well as Oshima *et al.*

Generally, a nanowire obtained simply by truncating its corresponding bulk is thermodynamically unstable. From the above analysis, the stable radii of a nanowire is quantum selective, and therefore it should be suggested that a nanowire must conform to these allowable magic radii by rearranging its inner atoms. Uncovering these rearranged structures of inner atoms is a challenge in both experimental techniques and theoretical modellings. It has been argued from experimental hints [19, 38], first-principles calculations [42], and molecular dynamics simulations [43], that a Au nanowire has a multishell structure composed of coaxial tubes and each tube consists of helical atom rows coiled round the wire axis. In addition, the helical structure is very close to a cylindrical geometry, as assumed in the present jellium model.

Now, we switch the discussion to nanomesas. In experiments wherein Au was deposited onto the HOPG surface [26], a Au nanomesa was found to grow both in its radius as well as in its height. So besides Eq. (4), another partial chemical potential needs to be introduced as [8, 39, 40]:

$$\mu_H = \left(\frac{\partial E}{\partial N}\right)_R = E_N - E_{N-1}|_{R=\text{constant}} \tag{6}$$

representing the change of energy with respect to changing the radius at a fixed height. A growth index function can then be defined as [39, 40]:

$$S(R,H) = \mu_H - \mu_R \tag{7}$$

which tells the energetically favored growth direction: $S(R,H) < 0$ indicates that at a given radius R and height H, the height growth is favored; $S(R,H) > 0$, the radial growth is favored. Thus, in order to determine the energetically favored Au nanomesa growth preference, a contour plot of the growth index S versus diameter D and height H is constructed, as shown in Fig. 3.

The main feature of Fig. 3(a) is that the S values (in units of eV) are basically divided into three different regions: orange, yellow, and green, which correspond to $S \approx -1$, $S \approx 0$, and $S \approx 1$, respectively. There is a clear asymptotic-like boundary between the orange and yellow regions, as well as between the yellow and green regions. From the definition of S, the orange region favors radial growth, and the green region favors height growth. When the mesa size is relatively small (1 nm $\lesssim D \lesssim$ 5 nm, and 1 nm $\lesssim H \lesssim$ 5 nm), the orange and green colors are generally symmetric about the $H = D$ line, indicating that radial growth and height growth are almost equally favorable. Such a growth feature in this size range is consistent with those observed in other experiments: a Au nanomesa on a HOPG surface can grow both in height and radius when its size is relatively small [26−28].

When $D \gtrsim 5$ nm, the colors of the pattern in Fig. 3(a) gradually become asymmetric with increasing size. A noticeable characteristic is that more and more discrete orange domains appear below the dashed $H = D$ line, and simultaneously, discrete green domains go down gradually toward the horizontal axis, as shown by arrows in Fig. 3(b), which, for clarity, is a magnification of the dashed red rectangular part in Fig. 3(a). Such charact-

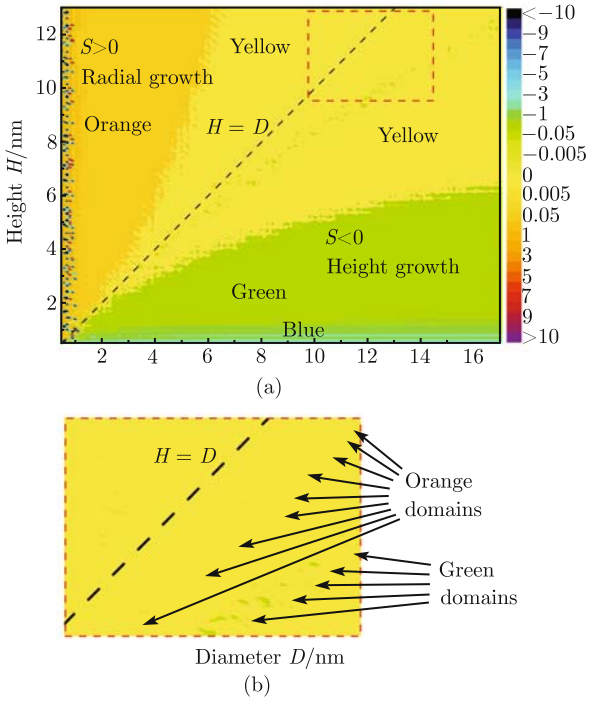

Fig. 3 **(a)** Contour plot of growth index S versus diameter D and height H for Au nanomesas. Colors and corresponding contrasts denote the values of S, which are in units of eV. **(b)** A magnification of the dashed red rectangular part in **(a)**. Arrows indicate some small discrete orange and green domains below the dashed $H = D$ line.

eristic of the growth index indicates that with increasing nanomesa size, the height growth is gradually hindered, while the radial growth becomes more favorable. This explains McBride *et al.*'s experimental observations: as the amount of Au deposited increases, the diameters of Au nanomesas will be larger and larger than their heights, which seem to be hindered [26]. According to McBride *et al.*'s experiments, an "optimal" height of ~ 11.4 nm appears when the lateral size of the Au nanomesa is large enough [26]. This is not in good agreement with the contour plot of Fig. 3, in which the height can be bigger than this value. The reason is possibly related to the substrate effect. Generally speaking, the substrate has a strong influence on the growth of nanomesas. Nevertheless, because graphite is a material that is known to interact weakly with many metals, the substrate effect has been neglected in the present model. However, when the lateral size of a Au nanomesa grown on the graphite surface (and therefore the interaction area between the mesa and the substrate) becomes larger, it is possible that the substrate may play a certain role so that the pattern of growth index will be correspondingly influenced. This can also be understood from the real mesa geometry in other experiments [26−28]: for a Au nanomesa, the area of its bottom face touching the substrate is a little bit larger than that of its top face due to the substrate effect.

When $D \lesssim 1$ nm, the growth index S has a big ruggedness, seen as a narrow region adjacent to the vertical axis in Fig. 3(a). This region contains many spots with different colors (red as well as blue) interspersed on an orange background like a jambalaya. This suggests a complex growth behavior of small-radius nanomesas, for which height growth and radial growth are alternately favored at different mesa sizes. In contrast, when $D \lesssim 1$ nm and $H \gtrsim 1$ nm, the growth index S exhibits some blue bands on a green background, as a narrow region adjacent to the horizontal axis in Fig. 3(a). This suggests that for small-height nanomesas with $D \lesssim 1$ nm, height growth is always favored over radial growth at all mesa sizes within this region.

Here it should be mentioned that in the present jellium model, the only parameter is the free electron density, or the corresponding Wigner-Seitz radius ($r_{\rm S}$). Calculations show that a small change in $r_{\rm S}$ does not result in a critical difference for the above discussion. Ag has nearly the same $r_{\rm S}$ as Au, and hence the results of Au can be qualitatively applied to Ag. There have been a few vacuum evaporation-deposition experiments reported for growing Ag nanomesas [44] but due to the lower coverage of Ag seen in other experiments [44], the Ag nanomesas are limited to small sizes. For this size region, it seems to be that the radial growth of a Ag nanomesa is slightly favored over its height growth, in little disagreement with the above discussion about Au nanomesas. No existing experiments with higher coverage of Ag are available, and experiments with higher coverage are suggested so that the results for a larger-sized region of Ag nanomesas can be compared.

Finally, it should be emphasized that the CHWJM is a very simple model, and it is impossible to accurately describe all the details regarding stability and growth behavior for an actual nanowire or nanomesa. The model could be extended by considering some theoretical modifications, e.g., the finiteness of the potential barrier U_0 in Eq. (1), interactions among ions and electrons, and some realistic experimental conditions, e.g., substrate effect, temperature effect, and nanostructure geometry. Nevertheless, as discussed above, the CHWJM can fairly reveal the essential physics of the studied problems, and the results from it should be useful as a rough guide in the research on metal nanostructures.

4 Conclusion

In conclusion, a cylindrical hard-wall jellium model

(CHWJM) was developed to investigate the stability of a Au nanowire and the preferred growth direction of a Au nanomesa for a broad-sized range containing hundreds to millions of atoms. Basic understanding of the QSE with regards to the formation of nanowires and nanomesas is demonstrated, and the most salient quantum features as observed in experiments are captured. The model shows that the radius of a Au nanowire is of quantum selectivity, being fairly consistent with the experimental results. It is suggested that the size selection of metal nanowires is mainly governed by quantum confinement effects during their formation, while a nanowire must conform to these quantum-mechanically allowable magic sizes by rearranging its inner atoms. The results from the model can also reasonably explain some puzzling behaviors in Au nanomesa growth experiments. The CHWJM can be also generally applicable to other metals.

Acknowledgements The author thanks Dr. Feng Liu, Dr. Cai-Zhuang Wang, and Dr. Elizabeth Lupton for helpful discussions. This work was supported by DOE-BES program. The calculations were performed on IBM SP RS/6000 at NERSC, and AMD Opteron cluster at the CHPC, University of Utah.

Appendix: Solution of Schrödinger equation with a cylindrical hard-wall potential

Assume that a single particle is enclosed in a cylindrical box with radius R and height H, as shown in Fig. 1(a), and in the cylindrical coordinates, the "hard wall" potential can be expressed as:

$$U=\begin{cases}0, & \text{for } 0<z<H, \text{ and } \rho<R\\ \infty, & \text{for } z<0, z>H, \text{ or } \rho>R\end{cases} \tag{A-1}$$

For $0\leqslant z\leqslant H$ and $\rho\leqslant R$, the wavefunctions satisfy the Schrödinger equation:

$$-\frac{\hbar^2}{2m^*}\nabla^2\psi(\rho,\varphi,z)=\epsilon\psi(\rho,\varphi,z) \tag{A-2}$$

where m^* is the effective mass of the particle. Let

$$k=\sqrt{\frac{2m^*\epsilon}{\hbar^2}} \tag{A-3}$$

and then Eq. (A-2) becomes

$$\nabla^2\psi+k^2\psi=0 \tag{A-4}$$

This is the Helmholtz equation. For $z\leqslant 0$, $z\geqslant H$, or $\rho\geqslant R$, the wavefunctions satisfy

$$\psi(\rho,\varphi,z)=0 \tag{A-5}$$

In cylindrical coordinates, Eq. (A-4) can be written as:

$$\frac{1}{\rho}\frac{\partial}{\partial\rho}\left(\rho\frac{\partial\psi}{\partial\rho}\right)+\frac{1}{\rho^2}\frac{\partial^2\psi}{\partial\varphi^2}+\frac{\partial^2\psi}{\partial z^2}+k^2\psi=0 \tag{A-6}$$

Assume that the solution of Eq. (A-6) has a factored form:

$$\psi(\rho,\varphi,z)=P(\rho)\Phi(\varphi)Z(z) \tag{A-7}$$

and then Eq. (A-6) can be written as:

$$\frac{\Phi Z}{\rho}\frac{\mathrm{d}}{\mathrm{d}\rho}\left(\rho\frac{\mathrm{d}P}{\mathrm{d}\rho}\right)+\frac{PZ}{\rho^2}\frac{\mathrm{d}^2\Phi}{\mathrm{d}\varphi^2}+P\Phi\frac{\mathrm{d}^2Z}{\mathrm{d}z^2}+k^2P\Phi Z=0 \tag{A-8}$$

Dividing Eq. (A-8) by $P\Phi Z$ and moving the z derivative term to the right-hand side yields

$$\frac{1}{\rho P}\frac{\mathrm{d}}{\mathrm{d}\rho}\left(\rho\frac{\mathrm{d}P}{\mathrm{d}\rho}\right)+\frac{1}{\rho^2\Phi}\frac{\mathrm{d}^2\Phi}{\mathrm{d}\varphi^2}+k^2=-\frac{1}{Z}\frac{\mathrm{d}^2Z}{\mathrm{d}z^2} \tag{A-9}$$

Then, a constant μ can be chosen to make

$$\frac{1}{\rho P}\frac{\mathrm{d}}{\mathrm{d}\rho}\left(\rho\frac{\mathrm{d}P}{\mathrm{d}\rho}\right)+\frac{1}{\rho^2\Phi}\frac{\mathrm{d}^2\Phi}{\mathrm{d}\varphi^2}+k^2=-\frac{1}{Z}\frac{\mathrm{d}^2Z}{\mathrm{d}z^2}=\mu \tag{A-10}$$

From the boundary condition

$$Z(0)=Z(H)=0 \tag{A-11}$$

the equation

$$-\frac{1}{Z}\frac{\mathrm{d}^2Z}{\mathrm{d}z^2}=\mu \quad \text{or} \quad \frac{\mathrm{d}^2Z}{\mathrm{d}z^2}+\mu Z=0 \tag{A-12}$$

has the solution

$$Z_n(z)=C_n\sin(lz), \quad l=\frac{n\pi}{H}, \quad n=1,2,\cdots \tag{A-13}$$

where C_n is an undetermined constant, and μ must be greater than zero so that another positive number l can be use to denote $\sqrt{\mu}$, which is allowed to take only the above discrete values. Thus, one equation in Eq. (A-10) can be written as:

$$\frac{1}{\rho P}\frac{\mathrm{d}}{\mathrm{d}\rho}\left(\rho\frac{\mathrm{d}P}{\mathrm{d}\rho}\right)+\frac{1}{\rho^2\Phi}\frac{\mathrm{d}^2\Phi}{\mathrm{d}\varphi^2}+k^2=\mu=l^2 \tag{A-14}$$

Multiplying Eq. (A-14) by ρ^2 and rearranging terms yields

$$\frac{\rho}{P}\frac{\mathrm{d}}{\mathrm{d}\rho}\left(\rho\frac{\mathrm{d}P}{\mathrm{d}\rho}\right)+(k^2-l^2)\rho^2=-\frac{1}{\Phi}\frac{\mathrm{d}^2\Phi}{\mathrm{d}\varphi^2} \tag{A-15}$$

Then, a constant λ can be chosen to make

$$\frac{\rho}{P}\frac{\mathrm{d}}{\mathrm{d}\rho}\left(\rho\frac{\mathrm{d}P}{\mathrm{d}\rho}\right)+(k^2-l^2)\rho^2=-\frac{1}{\Phi}\frac{\mathrm{d}^2\Phi}{\mathrm{d}\varphi^2}=\lambda \tag{A-16}$$

From the periodic boundary condition

$$\Phi(\varphi)=\Phi(\varphi+2j\pi), \quad j=0,\pm1,\pm2,\cdots \tag{A-17}$$

the equation

$$-\frac{1}{\Phi}\frac{\mathrm{d}^2\Phi}{\mathrm{d}\varphi^2}=\lambda \quad \text{or} \quad \frac{\mathrm{d}^2\Phi}{\mathrm{d}\varphi^2}+\lambda\Phi=0 \tag{A-18}$$

has the solution

$$\Phi_m(\varphi)=F_{-m}\mathrm{e}^{-\mathrm{i}m\varphi}+F_m\mathrm{e}^{\mathrm{i}m\varphi}, \quad m=0,1,2,\cdots \tag{A-19}$$

where F_m and F_{-m} are two undetermined constants, and λ must be equal to m^2. Therefore, in Eq. (A-16), the equation

$$\frac{\rho}{P}\frac{\mathrm{d}}{\mathrm{d}\rho}\left(\rho\frac{\mathrm{d}P}{\mathrm{d}\rho}\right)+(k^2-l^2)\rho^2=\lambda \tag{A-20}$$

can be expressed as:

$$\rho\frac{\mathrm{d}}{\mathrm{d}\rho}\left(\rho\frac{\mathrm{d}P}{\mathrm{d}\rho}\right)+\left[(k^2-l^2)\rho^2-m^2\right]P=0 \tag{A-21}$$

or

$$\frac{\mathrm{d}^2P}{\mathrm{d}\rho^2}+\frac{1}{\rho}\frac{\mathrm{d}P}{\mathrm{d}\rho}+\left[(k^2-l^2)-\frac{m^2}{\rho^2}\right]P=0 \tag{A-22}$$

Setting

$$x=\sqrt{k^2-l^2}\rho \tag{A-23}$$

and substituting Eq. (A-23) into Eq. (A-22), the Bessel differential equation is obtained as:

$$\frac{\mathrm{d}^2P}{\mathrm{d}x^2}+\frac{1}{x}\frac{\mathrm{d}P}{\mathrm{d}x}+\left(1-\frac{m^2}{x^2}\right)P=0 \tag{A-24}$$

which has the solution

$$P_m(\rho)=D_mJ_m(x) \tag{A-25}$$

with the condition

$$P_m(0)=\text{finite value} \tag{A-26}$$

Here, D_m is an undetermined constant. Combining Eqs. (A-3), (A-13), (A-19), (A-23), and (A-25), the wavefunctions are obtained as:

$$\begin{aligned}\psi_{mn}(\rho,\varphi,z)&=P_m(\rho)\Phi_m(\varphi)Z_n(z)\\&=A_{mn}J_m\left(\sqrt{\frac{2m^*\epsilon}{\hbar^2}-\frac{n^2\pi^2}{H^2}}\rho\right)\\&\quad\cdot\mathrm{e}^{\mathrm{i}m\varphi}\sin\frac{n\pi z}{H}\end{aligned} \tag{A-27}$$

where $m=0,\pm1,\pm2,\cdots$; $n=1,2,\cdots$, and

$$A_{mn}=C_nF_mD_m \tag{A-28}$$

These constants can be determined by the normalization conditions:

$$\int_0^H Z_n^*(z)Z_n(z)\mathrm{d}z=1 \tag{A-29}$$

$$\int_0^{2\pi}\Phi_m^*(\varphi)\Phi_m(\varphi)\mathrm{d}\varphi=1 \tag{A-30}$$

and

$$\int_0^R P_m^*(\rho)P_m(\rho)\rho\mathrm{d}\rho=1 \tag{A-31}$$

Now, consider the boundary condition

$$P_m(R)=0 \tag{A-32}$$

to obtain the energy eigenvalues. Substituting Eq. (A-25) into Eq. (A-32), and considering Eqs. (A-3), (A-13), and (A-23) together yields

$$J_m\left(\sqrt{\frac{2m^*\epsilon}{\hbar^2}-\frac{n^2\pi^2}{H^2}}R\right)=0 \tag{A-33}$$

which means that

$$\sqrt{\frac{2m^*\epsilon}{\hbar^2}-\frac{n^2\pi^2}{H^2}}R=Z_{m,\alpha} \tag{A-34}$$

where $Z_{m,\alpha}$ is the αth zero of the Bessel function $J_m(x)$. Thus, the energy at the quantum state $\psi_{m,\alpha,n}(\rho,\varphi,z)$, which is sometimes labelled as $|m,\alpha,n\rangle$ with the use of the Dirac symbol, can be written as

$$\begin{aligned}&\epsilon_{m,\alpha,n}=\frac{\hbar^2}{2m^*}\left(\frac{Z_{m,\alpha}^2}{R^2}+\frac{n^2\pi^2}{H^2}\right), \quad m=0,\pm1,\pm2,\cdots,\\&n=1,2,\cdots\end{aligned} \tag{A-35}$$

Here, the values of several zeroes of the Bessel function $J_m(x)$ are listed:

$$\begin{array}{lll}Z_{0,1}=2.4048, & Z_{0,2}=5.5201, & Z_{0,3}=8.6537,\cdots\\ Z_{1,1}=0.0000, & Z_{1,2}=3.8317, & Z_{1,3}=7.0156,\cdots\\ Z_{2,1}=0.0000, & Z_{2,2}=5.1356, & Z_{2,3}=8.4172,\cdots\\ Z_{3,1}=0.0000, & Z_{3,2}=6.3802, & Z_{3,3}=9.7610,\cdots\\ & \cdots\cdots & \end{array}$$

From the above values of zeroes, it is seen that $Z_{m\neq0,\,\alpha=1}=0$. Therefore, in order to guarantee that the wavefunctions do not vanish, one must have $\alpha=1,2,3,\cdots$, but $\alpha\neq1$ if $m\neq0$.

From the expressions of wavefuctions in Eqs. (A-13), (A-19), and (A-25) with the corresponding normalization conditions in Eqs. (A-29), (A-30), and (A-31), one can obtain

$$C_n=\sqrt{\frac{2}{H}}, \quad F_m=F_{-m}=\sqrt{\frac{1}{2\pi}}$$

and

$$D_m=D_{-m}=\frac{\sqrt{2}}{RJ_{m+1}(Z_{m,\alpha})} \tag{A-36}$$

and then from Eqs. (A-28), and (A-36), one can have

$$A_{mn} = \frac{\sqrt{2}}{R\sqrt{\pi H}J_{m+1}(Z_{m,\alpha})} \tag{A-37}$$

Substituting Eq. (A-37) into Eq. (A-27), the wavefuctions are obtained as:

$$\psi_{m,\alpha,n}(\rho,\varphi,z) = \frac{\sqrt{2}}{R\sqrt{\pi H}J_{m+1}(Z_{m,\alpha})} \cdot J_m\left(\sqrt{\frac{2m^*\epsilon}{\hbar^2} - \frac{n^2\pi^2}{H^2}}\rho\right) \mathrm{e}^{\mathrm{i}m\varphi} \sin\frac{n\pi z}{H} \tag{A-38}$$

Using Eq. (A-34), one can rewrite Eq. (A-38) as:

$$|m,\alpha,n\rangle \equiv \psi_{m,\alpha,n}(\rho,\varphi,z) = \frac{\sqrt{2}}{R\sqrt{\pi H}J_{m+1}(Z_{m,\alpha})} \cdot J_m\left(\frac{Z_{m,\alpha}}{R}\rho\right) \mathrm{e}^{\mathrm{i}m\varphi} \sin\frac{n\pi z}{H} \tag{A-39}$$

where $m = 0, \pm1, \pm2, \cdots; \alpha = 1, 2, 3, \cdots (\alpha \neq 1, \text{if } m \neq 0)$; and $n = 1, 2, 3, \cdots$.

References

1. M. L. Cohen and W. D. Knight, Phys. Today, 1990, 43(12): 42
2. W. A. de Heer, Rev. Mod. Phys., 1993, 65: 611
3. M. Brack, Rev. Mod. Phys., 1993, 65: 677
4. T. P. Martin, Phys. Rep., 1996, 273: 199
5. V. Lindberg and B. Hellsing, J. Phys.: Condens. Matter, 2005, 17: S1075
6. F. Liu, S. N. Khanna, and P. Jena, Phys. Rev. B, 1990, 42: 976
7. F. K. Schulte, Surf. Sci., 1976, 55: 427
8. Y. Han, J. W. Evans, and D.-J. Liu, Surf. Sci., 2008, 602: 2532
9. A. I. Yanson, I. K. Yanson, and J. M. van Ruitenbeek, Nature, 1999, 400: 144
10. A. I. Yanson, I. K. Yanson, and J. M. van Ruitenbeek, Phys. Rev. Lett., 2000, 84: 5832
11. A. I. Yanson, I. K. Yanson, and J. M. van Ruitenbeek, Phys. Rev. Lett., 2001, 87: 216805
12. M. Díaz, J. L. Costa-Krämer, E. Medina, A. Hasmy, and P. A. Serena, Nanotechnology, 2003, 14: 113
13. A. I. Mares, A. F. Otte, L. G. Soukiassian, R. H. M. Smit, and J. M. van Ruitenbeek, Phys. Rev. B, 2004, 70: 073401
14. A. I. Mares and J. M. van Ruitenbeek, Phys. Rev. B, 2005, 72: 205402
15. A. I. Mares, D. F. Urban, J. Bürki, H. Grabert, C. A. Stafford, and J.M. van Ruitenbeek, Nanotechnology, 2007, 18: 265403
16. A. I. Yanson and J. M. van Ruitenbeek, Phys. Rev. Lett., 1997, 79: 2157
17. I. K. Yanson, O. I. Shklyarevskii, J. M. van Ruitenbeek, and S. Speller, Phys. Rev. B, 2008, 77: 033411
18. T. W. Cornelius, M. E. Toimil-Molares, S. Karim, and R. Neumann, Phys. Rev. B, 2008, 77: 125425
19. Y. Kondo and K. Takayanagi, Science, 2000, 289: 606
20. C. A. Stafford, D. Baeriswy, and J. Bürki, Phys. Rev. Lett., 1997, 79: 2863
21. J. M. van Ruitenbeek, M. H. Devoret, D. Esteve, and C. Urbina, Phys. Rev. B, 1997, 56: 12566
22. C. Höppler and W. Zwerger, Phys. Rev. Lett., 1998, 80: 1792
23. D. F. Urban, J. Bürki, C.-H. Zhang, C. A. Stafford, and H. Grabert, Phys. Rev. Lett., 2004, 93: 186403
24. J. Bürki and C. A. Stafford, Appl. Phys. A, 2005, 81: 1519
25. D. F. Urban, J. Bürki, C. A. Stafford, and H. Grabert, Phys. Rev. B, 2006, 74: 245414
26. J. D. McBride, B. V. Tassell, R. C. Jachmann, and J. Thomas P. Beebe, J. Phys. Chem. B, 2001, 105: 3972
27. H. Hövel, Th. Becker, A. Bettac, B. Reihl, M. Tschudy, and E. J. Williams, J. Appl. Phys., 1997, 81: 154
28. H. Hövel, Th. Becker, A. Bettac, B. Reihl, M. Tschudy, and E. J. Williams, Appl. Surf. Sci., 1997, 115: 124
29. Y.-J. Zhu, A. Schnieders, J. D. Alexander, J. Thomas, and P. Beebe, Langmuir, 2002, 18: 5728
30. W. D. Knight, K. Clemenger, W. A. de Heer, W. A. Saunders, M. Y. Chou, and M. L. Cohen, Phys. Rev. Lett., 1984, 52: 2141
31. R. D. Woods and D. S. Saxon, Phys. Rev., 1954, 95: 577
32. K. Clemenger, Phys. Rev. B, 1985, 32: 1359
33. S. G. Nilsson, Mat.-Fys. Medd. Dan. Vidensk. Selsk., 1955, 29(16)
34. Y. Han, High Energ. Phys. Nucl., 2000, 24: 546
35. Z. Zhang, Q. Niu, and C.-K. Shih, Phys. Rev. Lett., 1998, 80: 5381
36. B. Wu and Z. Zhang, Phys. Rev. B, 2008, 77: 035410
37. G. Mills, B. Wang, W. Ho, and H. Metiu, J. Chem. Phys., 2004, 120: 7738
38. Y. Oshima, A. Onga, and K. Takayanagi, Phys. Rev. Lett., 2003, 91: 205503
39. Y. Han, J. Y. Zhu, F. Liu, S.-C. Li, J.-F. Jia, Y.-F. Zhang, and Q.-K. Xue, Phys. Rev. Lett., 2004, 93: 106102
40. Y. Han and F. Liu, Front. Phys. China, 2008, 3(1): 41
41. E. Ogando, N. Zabala, and M. J. Puska, Nanotechnology 2002, 13: 363
42. R. T. Senger, S. Dag, and S. Ciraci, Phys. Rev. Lett., 2004, 93: 196807
43. J.-S. Lin, S.-P. Ju, and W.-J. Lee, Phys. Rev. B, 2005, 72: 085448
44. I. Lopez-Salido, D. C. Lim, and Y. D. Kim, Surf. Sci., 2005, 588: 6